Single substitutional nitrogen defects revealed as electron acceptor states in diamond using ultrafast spectroscopy

R. Ulbricht and S. T. van der Post
FOM Institute AMOLF, Amsterdam, Science Park 104, 1098 XG Amsterdam, The Netherlands

J. P. Goss and P. R. Briddon
School of Electrical, Electronic and Computer Engineering, Newcastle University, Newcastle upon Tyne, NE1 7RU, UK

R. Jones
Department of Physics, University of Exeter, Exeter EX4 4QL, UK

R. U. A. Khan
DTC Research Centre, Maidenhead, Berkshire, SL6 6JW, UK

M. Bonn*
FOM Institute AMOLF, Amsterdam, Science Park 104, 1098 XG Amsterdam, The Netherlands and
Max Planck Institute for Polymer Research, Ackermannweg 10, 55128 Mainz, Germany
(Received 1 June 2011; revised manuscript received 1 September 2011; published 3 October 2011)

We report on the carrier dynamics and recombination pathways of photogenerated electrons in type Ib synthetic diamond using ultrafast spectroscopic techniques. Samples with controlled amounts of nitrogen defects were grown using the high-pressure high-temperature (HPHT) method. Electrons were excited from single substitutional nitrogen defects into the conduction band via an ultrashort pulse from a frequency-doubled Ti-sapphire laser. Using time-resolved terahertz time-domain spectroscopy, we determined the mobility of the photoexcited electrons and monitored their recombination dynamics, at temperatures ranging from cryogenic temperatures to room temperature. The electron mobility was observed to be limited by scattering with neutral nitrogen impurity defects (N_s^0). Electrons were observed to predominantly recombine into neutral nitrogen states rather than their original ionized nitrogen defects, thereby creating negatively charged nitrogen states (N_s^-). The creation of N_s^- states is confirmed experimentally by tracking the localized vibrational modes (LVM) of nitrogen defects during the electron recombination process using visible pump-infrared probe transient spectroscopy. We observe a transient infrared absorption feature at 1349 cm^{-1} that can be assigned to the LVM of N_s^-. Density functional calculations are carried out to determine the LVMs of nitrogen in various charge states, and we find a $\sim$10 cm^{-1} upward shift of the mode on passing from N_s^0 to N_s^-, in agreement with experimental observations.

DOI: 10.1103/PhysRevB.84.165202 PACS number(s): 78.47.D−, 78.30.Am, 72.20.Jv

I. INTRODUCTION

Diamond is a versatile material that shows exceptional promise in a range of optical, quantum optical, and electronic applications.[1–4] There are two main methods by which synthetic diamond may be grown: high-pressure high-temperature (HPHT) synthesis and chemical vapor deposition (CVD). In both cases, the dominant impurity in diamond is single substitutional nitrogen (N_s), which is known to act as a deep donor approximately 1.7 eV below the conduction band.[5]

The optoelectronic transitions associated with the N_s defect have important implications for several potential applications of diamond. First, N_s defects act as electron traps, thereby significantly limiting the performance of diamond-based devices that may potentially be used as detectors or for high-power electronics. Understanding the influence of traps on relevant figures of merit of charge carriers such as their mobility and lifetime is thus important. Second, the negatively charged nitrogen vacancy defect (NV^-) is currently being intensively studied for spintronics.[6,7] The existence of this defect is dependent on electrons being donated from single nitrogen to neutral nitrogen vacancy (NV) defects. One of the most significant issues with NV^- centers as stable quantum emitters is the phenomenon of "blinking," which may be a result of instability in the charge state of the NV defect. Previous theoretical studies[8] have suggested that N_s may act not only as an electron donor, which is intuitive given its valency, but also as an acceptor. If so, this would have important implications, for example, to compensate phosphorus donors, which may be incorporated into CVD synthetic diamond to produce *n*-type devices[9] and potentially also to convert NV^- centers back to their neutral state. However, there has been no experimental evidence for the electron-accepting property of N_s so far, i.e., for the possibility that N_s defects become negatively charged. This is likely due to the challenge of detecting this state spectroscopically; it is presumably unstable and thus short lived. Time-resolved techniques that are able to probe electron and defect-charge dynamics on ultrafast time scales can potentially offer a means to achieve this goal.

In this study, we report on the transport properties and picosecond time scale relaxation dynamics of electrons excited from N_s defects into the conduction band in HPHT-grown type Ib diamond. The investigated samples contain a controlled concentration of N_s defects of the order of hundreds of parts per million and negligible amounts of other unintentional dopants.

Using time-resolved terahertz spectroscopy, we measure the mobility of the donor-excited electrons and the time scale of their back-recombination from the conduction band as a function of N_s concentration, ionized impurity density, and temperature. The recombination dynamics show a clear dependence on the neutral rather than the ionized impurity concentration, suggesting that electrons do not only relax back into the photoionized defects but also into neutral N_s states. This strongly suggests that N_s can act as an acceptor state, forming negatively charged N_s defects (N_s^-). The presence of this remarkable relaxation channel is confirmed by independent measurements on the same diamond samples using time-resolved infrared spectroscopy with which we probe the localized vibrational modes (LVM) of defects within diamond. Here, the appearance of negatively charged nitrogen defects following optical excitation manifests itself through a transient IR absorption feature of the LVM at 1349 cm^{-1}. Density functional theory calculations confirm this assignment.

II. METHODS

Standard high-pressure high-temperature (HPHT) grown type Ib synthetic diamond samples were investigated in this study. As-grown HPHT synthetic diamond material from three different growth runs was processed into thin plates of dimensions of approximately $5\times5\times0.5$ mm, using laser sawing and polishing. Each plate possessed a main face corresponding to the $\{100\}$ surface. For all of these samples, the central region of the main face corresponded to the $\{100\}$ growth sector, and only this sector was probed in the experiments reported here.

By performing room temperature UV-visible absorption measurements on these samples and comparing the resulting absorption spectra to that of a diamond sample with a known neutral single substitutional nitrogen (N_s^0) concentration,[10] it was possible to determine the N_s^0 concentration of the central growth sectors. We investigated three samples with concentrations of 100, 150, and 300 (±10) ppm, respectively. The central $\{100\}$ growth sectors are expected to possess negligible concentrations of other defects, besides single nitrogen.

Time-resolved terahertz time-domain spectroscopy as a probe of charge carrier dynamics has been described extensively in the literature.[11,12] The setup used for this experiment utilizes an amplified Ti:Sapphire laser operating at a repetition rate of 1 kHz, delivering pulses with a duration of 150 fs and an energy of 1 mJ at a wavelength of 800 nm. Ninety percent of the output energy is split off and used as the excitation pulse by frequency doubling it to a wavelength of 400 nm (3.1 eV) with a Beta barium borate (BBO) crystal. The remaining output is used to generate and detect terahertz radiation. The terahertz radiation is generated via optical rectification in a 1-mm-thick ZnTe crystal and detected via electro-optic sampling in a second ZnTe crystal of the same dimensions.[13] A cryostat (Oxford Instruments, Optistat AC-V12) is used to cool the sample to temperatures down to 10 K. The generated terahertz probe spectrum covers a broad frequency range spanning from 0.3 to 2 THz. One particular feature of the electro-optic detection method is that it works in the time domain, i.e., it records the time-dependent electric field of the terahertz probe pulse, rather than the time-integrated intensity. As opposed to most conventional spectrometers based on intensity measurement, this implies that not only the absorption spectrum of the sample can be detected. Also changes in the phase can be resolved over the whole pulse bandwidth. As a result, not only the absorption but also the refractive index changes of the investigated material can be inferred, i.e., the complete complex refractive index. By modulating the excitation beam with an optical chopper and recording the difference signal using a lock-in amplifier, we determine the excitation-pulse-induced terahertz response, i.e., the change of the complex index of refraction of diamond due to the presence of photoexcited charge carriers.

The setup for the visible pump-infrared probe measurements is driven by another amplified Ti:Sapphire laser system. It delivers pulses with durations of 50 fs and energies of 3 mJ. Thirty percent of the output is split off and frequency doubled in a BBO crystal to photoexcite the sample with light at a wavelength of 400 nm (3.1 eV). The remaining output is used to drive an optical parametric amplifier (OPA), after which the midinfrared probe light is generated by difference-frequency mixing of the signal and idler beams from the OPA in a $AgGaS_2$ crystal. The probe pulse is centered at a frequency of 1340 cm^{-1} (=165 meV) and has a bandwidth of 350 cm^{-1} (=40 meV). After transmission through the sample, the probe pulse is spectrally dispersed using an Oriel MS260i grating spectrometer and detected using a 32-channel Mercury-Cadmium-Telluride (MCT) detector array.

For the calculations of the LVM, we use a spin-density-functional package, as implemented in AIMPRO[14,15] with both local density[16] and generalized gradient[17] approximations (LDA and GGA). Point defects are modeled using a supercell approach, where individual defects are approximated by a crystal of well-spaced defects. In order to estimate the impact of the periodic boundary conditions on the derived quantities, we have used simple cubic supercells of side length $3a_0$ and $4a_0$, containing 216 and 512 host atoms, respectively. The wave function basis consists of atom-centered Gaussians.[18] The charge density is Fourier transformed using plane waves with a cutoff of 350 Ry, yielding well-converged total energies. Core electrons are included through norm-conserving pseudopotentials.[19]

Within the LDA and GGA approaches, the lattice constant and bulk modulus of bulk diamond are reproduced well in comparison to experiment. In the LDA (GGA) a_0 is underestimated (overestimated) by $\sim1\%$ (0.2%), and B_0 is overestimated(underestimated) by 6% (0.5%). The calculated direct and indirect band gaps agree with published plane-wave values,[20] and the basic methodology has been tested on many defects in diamond[21] and other materials.

In all cases we sample the Brillouin zone using the Monkhorst-Pack scheme,[22] a $2\times2\times2$ for the 216 atom cells, and a Γ-point approximation for the 512 atom cell. These correspond to sampling densities of 0.025 and 0.085 points per $Å^{-3}$, respectively. For the simulation of vibrational modes, the second derivative of the total energy with respect to displacement of the atoms is obtained using a finite difference approximation using the analytic forces. A quasiharmonic dynamical matrix is then built in the usual way, and diagonalization yields vibrational frequencies. For each supercell size, the frequencies have been obtained (a) under the constraint

that the lattice constant is that of the corresponding defect-free supercell and (b) where a zero pressure boundary condition has been applied so that the lattice constant is freely varied to minimize the total energy.

III. RESULTS AND DISCUSSION

The absorption spectrum of the 100-ppm sample is shown in Fig. 1(a). The origin of the absorption peak at 4.5 eV (270 nm) is still under debate. One possible mechanism, as will be discussed further down, relates it to a transition between the valence band and the N_s^- defect state whose existence is shown in this work.[8]

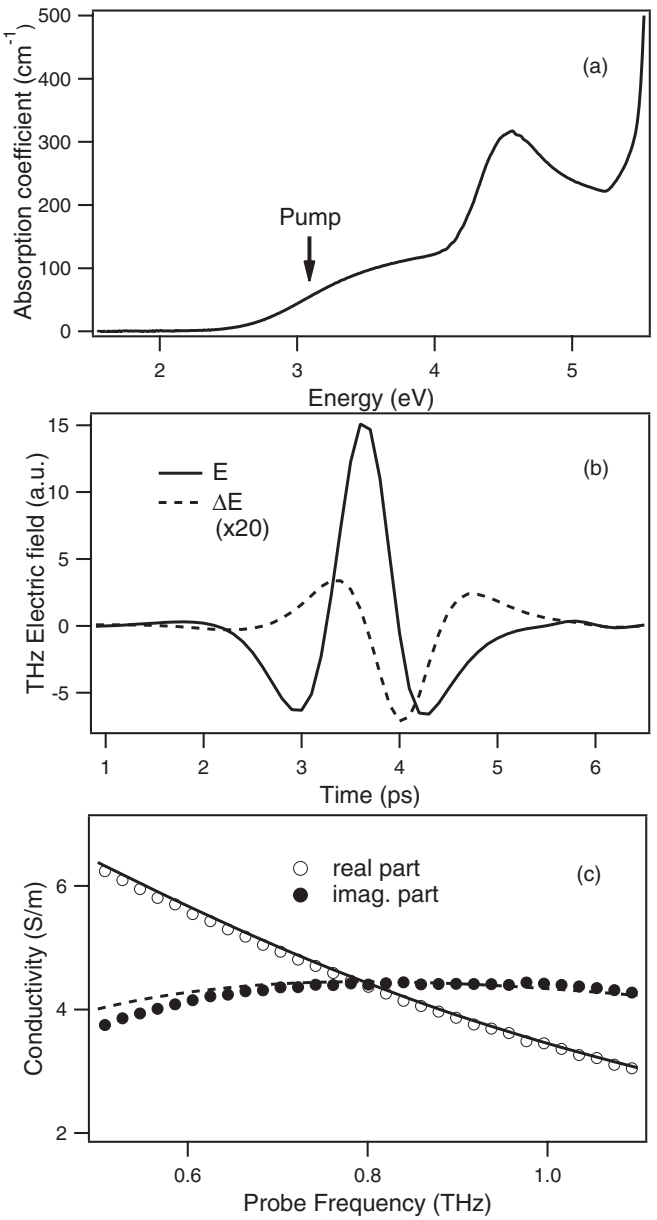

FIG. 1. (a) shows the absorption spectrum of the 100-ppm sample. The excitation energy of 3.1 eV is indicated with an arrow; (b) shows the recorded terahertz field E transmitted through the unexcited diamond sample at 200 K (solid line) and the photomodulated terahertz field ΔE (dashed line) in the time domain; (c) shows the extracted complex photoconductivity in the frequency domain (circles) and the obtained fit to the Drude model that yields an electron scattering time of 200 fs (solid and dashed lines). The measurements were taken at a pump-probe delay of 2 ps.

In all of the pump-probe spectroscopy measurements that are presented in the following, electrons are excited from neutral nitrogen (N_s^0) states into the conduction band by pump pulses with photon energies of 3.1 eV [400-nm wavelength, indicated with an arrow in Fig. 1(a)], as was shown in Ref. 5. This creates hot electrons with initial excess energies of around 1.4 eV that subsequently relax to the bottom of the conduction band within less than 2 ps. All spectra presented here have been recorded after that point.

In the following, we express the complex index of refraction of the excited electrons measured by our terahertz spectrometer in terms of the complex conductivity. The complex index of refraction $\hat{n}$ of a material is related to the complex dielectric function $\hat{\varepsilon}$ via $\hat{\varepsilon} = \hat{n}^2$, The complex conductivity $\hat{\sigma}$ of the photoexcited electrons can then be derived through $\hat{\sigma} = -i\omega\varepsilon_0(\hat{\varepsilon} - \hat{\varepsilon}_\infty)$, where ω is the angular frequency, ε_0 the free-space permittivity, $\hat{\varepsilon}$ the dielectric constant of the photoexcited diamond, and $\hat{\varepsilon}_\infty$ the dielectric constant of the unexcited diamond. In the actual terahertz measurement, both the transmission of the terahertz probe through the unexcited sample $E(t)$ and the pump-induced transmission change $\Delta E(t)$ are recorded in the time domain, as shown in Fig. 1(b). The ratio ΔE(t)/E(t) is then used to extract the complex conductivity $\hat{\sigma}(\omega)$ following the procedure described in Ref. 23. We determined the terahertz conductivities of all three samples at different temperatures between 10 K and room temperature immediately after all electrons had relaxed to the bottom of the conduction band. Excitation fluences were chosen such that the density of the excited electron plasma was on the order of 10^{14} cm^{-3}. The conductivity spectra were fitted by the Drude model Ref. 24—a Lorentzian oscillator centered at zero frequency:

$$\hat{\sigma}(\omega) = \frac{Ne^2\tau/m^*}{1 - i\omega\tau}. \quad (1)$$

Here, N denotes the photoexcited electron density, e the unity electron charge, m^* the electron effective mass (taken to be 0.36 m_e, where m_e denotes the electron rest mass[25]), and τ the electron scattering time. The linewidth of this Drude resonance is defined by the scattering rate $1/\tau$. Figure 1(c) shows an exemplary Drude fit for the photoconductivity measured at 200 K, yielding a scattering time of 200 fs, which showed no significant dependence on the pump-probe delay time. It is evident from the comparison of the data with the fit in Fig. 1(c) that two adjustable parameters (density N and scattering rate $1/\tau$) are sufficient to accurately describe the frequency-dependent photoconductivity.

Figure 2 shows the extracted electron scattering times for all three diamond samples at various temperatures and their corresponding mobility values μ, related to the scattering time through $\mu = e\tau/m^*$. The excited electron density is determined by the excitation photon flux and the absorption cross section at 400 nm. The optical properties have been verified not to change significantly with varying temperature; the photon flux was kept equal for all measurements to achieve a photoexcited electron density of 3^*10^{14} cm^{-3}. Hence the

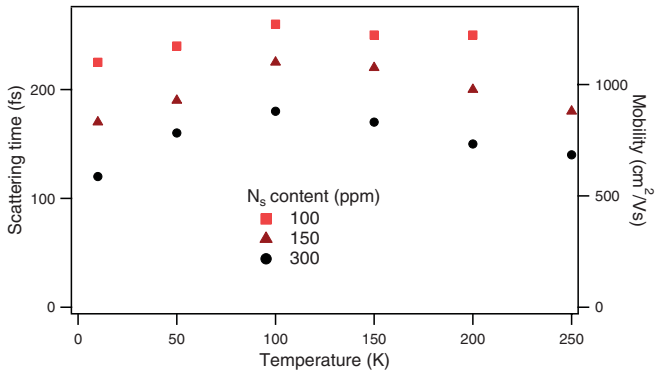

FIG. 2. (Color online) Temperature dependence of the electron scattering time τ (left axis) and mobility μ (right axis) for all three measured diamond samples possessing different concentrations of single substitutional nitrogen defects. All the data was taken at fixed photoexcited carrier density of $3^{*}10^{14}$ cm^{-3} at a delay time of 2 ps after photoinjection of carriers.

electron density does not vary for the measurements shown in Fig. 2. It is further evident that as free electrons are generated through ionization of single nitrogen atoms, the density of resulting ionized, positively charged, nitrogen states (N_s^+) is equally constant. From Fig. 2 it is observed that the electron mobility is only weakly dependent on temperature for all three samples, with values around 1000 cm^2/Vs. More precisely, it increases by approximately 30% when the temperature is raised from 10 to 100 K, from where it decreases again by the same amount upon further increasing the temperature to 250 K. This temperature dependence of the mobility is distinctly different from the one commonly observed in high-purity diamond. In high-purity diamond, the electron mobility decreases continuously with increasing temperature. Hall measurements,[26] time-of-flight,[25] photoconductivity,[4] and light-induced transient grating experiments[27] on such diamond samples have shown that the electron mobility follows a $T^{-3/2}$ dependence below room temperature, which is characteristic for acoustic-phonon scattering, reaching values up to several thousand cm^2/Vs at cryogenic temperatures. In doped type Ib diamond, however, other scattering mechanisms are likely to make a contribution in addition to phonon scattering, namely scattering with neutral and photoionized (positively charged) nitrogen defects. Figure 2 reveals that a higher N_s^0 defect concentration indeed reduces the total mobility over all temperatures measured. Because the excited electron density and thus the density of ionized impurities in these measurements were kept constant between the samples by adjusting the excitation fluence, this result suggests that the scattering contribution from neutral nitrogen defects is substantial. This is not surprising: although the scattering cross section of charged impurities is generally orders of magnitude larger than neutral ones,[28] according to the excitation fluences used in our measurements, only about 1 out of 10^5 nitrogen defects is ionized. Hence the vast majority of nitrogen defects are still neutral, contributing substantially to carrier scattering. The temperature dependence of the mobility supports this picture: the simplest model to describe scattering by neutral impurities predicts that the mobility is temperature independent,[29] as largely borne out by the experimental results. We note that similar behavior has been observed previously in a boron-doped diamond.[30] The contribution from scattering off ionized impurities becomes evident in our measurements at higher excitation densities (data not shown). It remains rather limited, however: an increase of the electron density by more than an order of magnitude, from $1^{*}10^{14}$ cm^{-3} to $2^{*}10^{15}$ cm^{-3}, resulted in a reduction of the mobility by only 20%. Approaching room temperature, the scattering rate by acoustical phonons becomes comparable to defect scattering, i.e., acoustical phonon scattering is increasingly likely to contribute to the total scattering rate. This would explain the observed mobility decrease at temperatures above 100 K.

To conclude this section, our findings qualitatively suggest that the electron mobility in a N-doped diamond is predominantly limited by scattering from N_s^0 defects, with additional contributions from N_s^+ defects and acoustical phonons that become more dominant at larger N_s^+ densities and higher temperatures, respectively.

In the following, we focus on the dynamics of recombination of the photoexcited electrons from the conduction band. A discussion about the physical mechanism will follow at a later stage of this report. In order to investigate the electron recombination, we monitor the decay of the real part of the conductivity at a fixed probe frequency as a function of pump-probe delay t_{pump}. According to the Drude model, the real conductivity scales with $\mathrm{Re}(\hat{\sigma}, t_{\mathrm{pump}}) \sim N(t_{\mathrm{pump}})\tau$. We experimentally verified that τ does not change significantly during the recombination process by taking terahertz conductivity spectra during the relaxation process and extracting the scattering time from them. Hence, $\mathrm{Re}(\hat{\sigma}, t_{\mathrm{pump}}) \sim N(t_{\mathrm{pump}})$, and we can use the real conductivity as a direct probe of the time-dependent electron density.

Figure 3(a) shows the time dependence of the real part of the conductivity, reflecting the variation of electron density in time, for all three samples at room temperature. The photogenerated electron density, and thus the photogenerated N_s^+ density, was kept constant at a value of $3^{*}10^{14}$ cm^{-3}. All dynamics show a modest speed-up of the decay with increasing pump-probe delay time, but the dynamics can be approximated very well by single exponential decay, which can be recognized as a linear slope in the logarithmic plot shown in Fig. 3(a). Electrons relax from the conduction band on a time scale of several tens of picoseconds, with a recombination time τ_r that decreases for higher N_s defect concentrations. We note that another study on type Ib diamond using a light-induced transient grating technique has recently found similar relaxation behavior related to single substitutional nitrogen.[31] The authors observed nonexponential recombination dynamics on time scales of several hundred picoseconds. However, they were using excitation pulses at a wavelength of 213 nm, which creates electrons *and* holes through interband excitation, which complicates the dynamics. We like to stress that the 400-nm excitation pulse employed here only excites electrons from N_s defects. Figure 3(b) summarizes the τ_r data for all three samples at various measured temperatures. τ_r increases with increasing temperature until it levels off at 150–200 K. A model describing the temperature dependence of the recombination kinetics in terms of the temperature-dependent scattering rate and thermal velocity will be presented below. Remarkably, τ_r is almost inversely proportional to the N_s

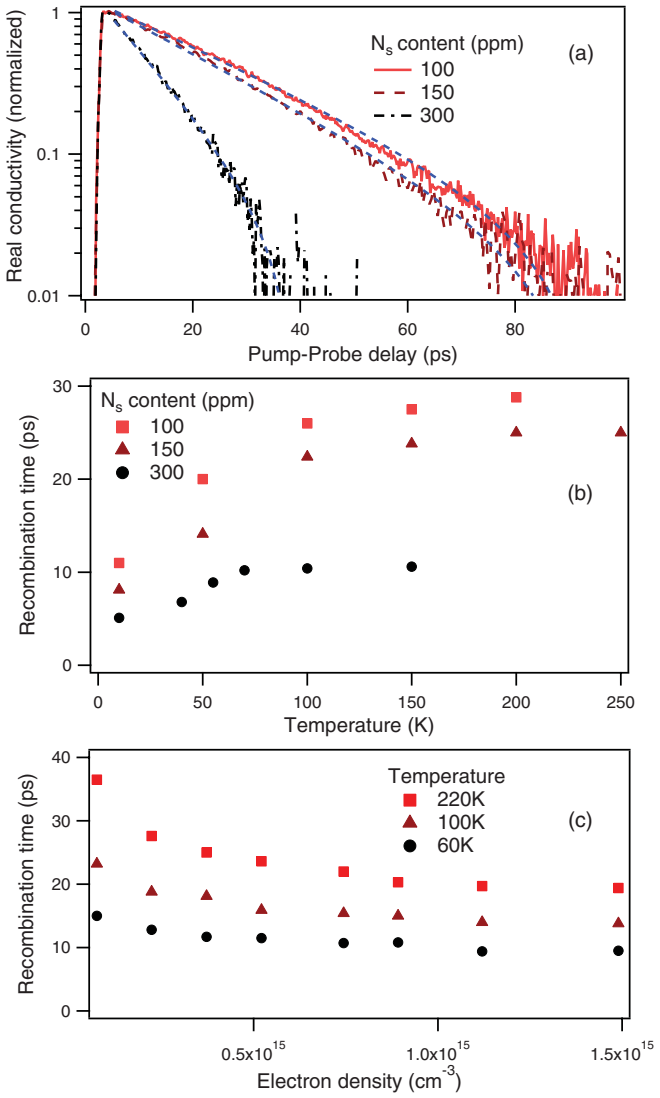

FIG. 3. (Color online) Electron recombination dynamics as measured by terahertz spectroscopy; (a) logarithmic plot of the temporal evolution of the normalized terahertz real conductivity (proportional to the free electron density) at room temperature for three diamond samples with different N_s concentrations; the slopes of the decays (obtained from single exponential fits shown as dotted lines), proportional to the recombination rate $1/\tau_r$, show a strong dependence on N_s concentration; (b) shows the temperature dependence of the extracted recombination times τ_r for all three samples (data for both graphs was recorded at fixed photoexcited carrier density of $3*10^{14}$ cm^{-3}); and (c) the dependence of τ_r on the photoexcited electron density for the sample with N_s concentration of 150 ppm at temperatures 60, 100, and 220 K.

concentration, particularly at high temperatures: a three times larger N_s concentration reduces τ_r by a factor of 2.5 above 150 K. Since the N_s^+ density due to photoexcitation from defect states is equal for the different samples, the observed inverse proportionality between N_s and τ_r strongly suggests that most electrons relax into N_s^0 states rather than their original N_s^+ states. That would imply that negatively charged nitrogen states (N_s^-) are formed. Akin to the scattering cross section, the capture cross section of a positively charged defect is generally larger than its neutral state value,[32] but again, the presence of a vast majority of N_s^0 defects would be dominant in this case. Consequently, similar to the mobility behavior discussed above, the influence of N_s^+ states becomes more pronounced at higher N_s^+ densities, i.e., higher incident fluences, also resulting in higher electron densities. Figure 3(c) shows the dependence of τ_r on the electron (i.e., N_s^+) density in the 150-ppm sample for three different temperatures. As expected, the relaxation time decreases with increasing electron density. Assuming a 1:1 ratio for the N_s^+ : electron density, N_s^+ states are increasingly able to scavenge electrons at higher densities. However, this effect is again weaker than the dependence on the N_s^0 concentration. As can be seen from Fig. 3(c), a 15-fold increase of the N_s^+ density results in a decrease of τ_r by only 30 to 40%. The recombination dynamics display single exponential behavior in all cases.

To test the hypothesis that electrons mainly recombine at neutral nitrogen defects, we made use of the fact that single substitutional nitrogen defects exhibit LVM, which give rise to sharp absorption lines in the infrared part of the electromagnetic spectrum. Additionally, the spectral position of the vibrational mode depends on the charge state of the defect. Figure 4(a) shows a Fourier transform infrared (FTIR) spectrum of one of the investigated samples. A sharp absorption peak can be seen at 1344 cm^{-1} that is characteristic for N_s^0 defects.[33] The broad background on the lower wave number side of the spectrum is also N_s^0 related (i.e., its intensity scales with the N_s^0 resonant feature). It has been shown that N_s^+ states exhibit an absorption peak at 1332 cm^{-1}.[33] Spectral signatures of negatively charged single substitutional nitrogen states have not been observed so far. By monitoring the temporal evolution of the IR spectrum after photoexcitation, it was possible to observe time-dependent absorption changes of the vibrational modes.

Figure 4(b) shows the pump-induced transmission changes T/T_0 of the IR spectrum measured on the 300-ppm sample from the point of photoexcitation up to a pump-probe delay of 30 ps, with an excitation photon flux resulting in an electron density of $4*10^{15}$ cm^{-3}. In the ratio T/T_0, T is the transmission through the excited sample and T_0 the transmission through the unexcited sample. Thus, $T/T_0 < 1$ indicates pump-induced absorption and $T/T_0 > 1$ pump-induced bleaching. The broad absorption feature shown in Fig. 4(b) originates from the high-frequency tail of the Drude response of the excited electrons. It vanishes on a time scale that is comparable with the charge carrier decay time in the terahertz measurements. On top of this broad absorption, a variety of absorption and bleach features are visible. These features are not sample related but are artifacts due to the presence of water vapor in the setup. The vibrational modes of free water exhibit several sharp absorption resonances at the spectral positions of these features. The absorption signatures from the water vapor that the probe pulse acquires during propagation interfere with the broad charge carrier response, resulting in the observed absorption and bleach effects around these resonances. This phenomenon is somewhat reminiscent of the Fano effect.[34]

Even though the measurement chamber had been flushed with nitrogen in order to reduce the humidity to close to zero, this effect could not be removed completely. Because the anticipated transient signals are on the order of 1/1000

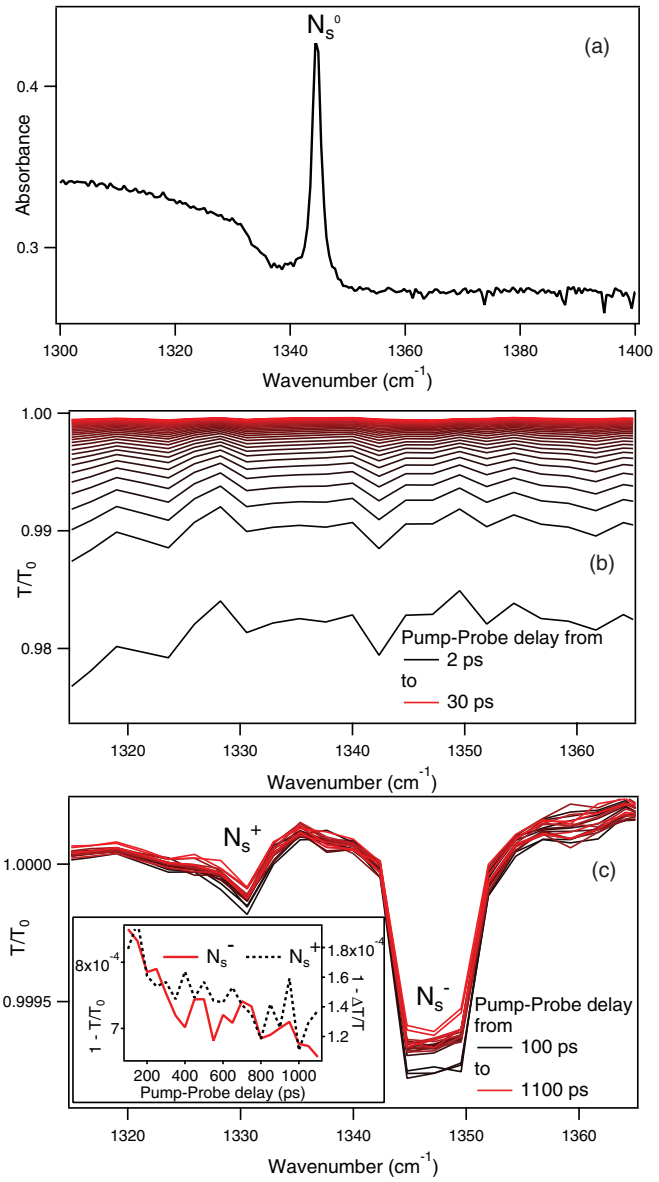

FIG. 4. (Color online) (a) FTIR spectrum of the 300-ppm type Ib diamond sample showing an absorption peak at 1344 cm^{-1}, which is due to the LVM of N_s^0 defects; (b) transient IR measurements in the same spectral region during electron recombination for pump-probe delays from 2 ps to 30 ps; (c) transient IR measurements after all electrons have recombined, for pump-probe delays between 100 ps and 1100 ps. The two visible peaks are assigned to the LVM of N_s^+ (left, centered at 1332 cm^{-1}) and N_s^- (right, centered at 1349 cm^{-1}). The inset shows the decay of the amplitude of both peaks in the same time frame.

and less and thus much smaller than the artifacts, we cannot draw any conclusions from this short-time data set regarding the presence of (charged) nitrogen sites.

Fortunately, the artifacts disappear when the background, due to the electron Drude response, vanishes, i.e., all electrons have relaxed from the conduction band. Figure 4(c) shows the temporal evolution of the IR signal over the wave number range investigated from a pump-probe delay of 100 ps to 1100 ps. Two main pump-induced absorption peaks are visible. One of these is at 1332 cm^{-1} and has been attributed to the N_s^+ defect Ref. 33. This is as expected if neutral nitrogen acts as a charge acceptor, as therefore not all photoelectrons in the conduction band would then recombine with photoionized nitrogen defects. Hence some nitrogen defects will remain positively charged. The results are therefore consistent with the assumption that a proportion of the photoelectrons have recombined with N_s^0 rather than N_s^+ defects. Looking at the figure, we also observe a second, more prominent transient IR peak at (1349 ± 0.5) cm^{-1}. Our analysis suggests that this feature is the LVM of the created N_s^- states. In principle one would also anticipate to observe in Fig. 4(c), in addition to the LVM's from the N_s^+ and N_s^- states, a bleaching response of the N_s^0 peak because these states are now depopulated as compared to the equilibrium case. However, its absorption cross section is seven times smaller than the N_s^+ peak, and this bleaching effect is thus invisible in the experiment.[33]

In order to provide theoretical support to our hypothesis that the observed transient absorption peak at 1349 cm^{-1} is indeed a LVM of N_s^-, we carried out density functional calculations of the local vibrational modes of N_s in various charge states.

Some of us have previously shown that, although the positively charged substitutional nitrogen defect N_s^+ is a tetrahedral center, N_s^0 is a trigonal center with one unique N-C bond elongated by about 30%.[8,35] The resulting shortening of the unique carbon back bonds leads to a local vibrational mode at 1344 cm^{-1}, which is insensitive to the nuclear mass of nitrogen in agreement with experiment.[36] However, there is a change in lattice parameter arising from the high concentrations of nitrogen in the lattice, and this has a pronounced effect on the local mode frequency.[37] Here we compare the calculated shift in the vibrational mode of N_s^- relative to that of N_s^0 by taking into account this change in lattice parameter. That is, we calculate the blueshift in the LVM resulting from negatively charging the N_s^0 defect.

In all cases, we find that there is a local mode above the one-phonon maximum, which is doubly degenerate, and therefore transforms as E in the C_{3v} point group. The calculated blueshift in frequency with change of charge state for the three cell sizes and boundary conditions are listed in Table I. For the negative charge state, the impact upon the lattice constant is greater than that for the neutral charge state so that the boundary condition has a larger impact upon the relative frequencies in the smaller unit cell than in the larger.

Although there is scatter in the relative location of the N_s^- mode to that of the neutral charge state, the average shifts for the LDA and GGA calculations are around 13 and 10 cm^{-1},

TABLE I. Local mode frequency of N_s^- minus that of N_s^0 (cm^{-1}). L is the length of the cubic supercell in each case, and LDA and GGA refer to the functional used, as described in Sec. II. Bulk and relaxed refer to the cell volume boundary conditions being fixed at that calculated for bulk diamond and that in which the lattice constant is varied to minimize the total energy, respectively.

	LDA		GGA	
L	Bulk	Relaxed	Bulk	Relaxed
$3a_0$	16	7	13	6
$4a_0$	16	12	12	8

respectively. Noting that the experimental value for the local mode of N_s^0 is 1344 cm^{-1}, this places an estimate for the local mode of N_s^- around 1354–1357 cm^{-1}, about 5–8 cm^{-1} larger than the experimentally determined value of 1349 cm^{-1}. It is evident, however, that these calculations qualitatively confirm the 1349 cm^{-1} resonance as being due to the N_s^- defect.

The question presents itself how, after an electron is captured by a neutral N_s^0 defect, the resulting N_s^- defect population returns to equilibrium, i.e., how N_s defects return to their neutral charge state and on what time scales this occurs. In the inset of Fig. 4(c), we plot the temporal evolution of the N_s^+ and N_s^- peak values, $1-T/T_0$, over the course of one nanosecond after photoexcitation. Although there is significant scatter in the data, the peak amplitudes of the two resonances are observed to decrease over this time scale. These data points were corrected for broad offsets in order to avoid the introduction of artificial trends. Spectral data points adjacent to the absorption peaks did not show a temporal decay of T/T_0 but stayed constant as expected, again confirming that the decay of the two peak decays is real. Although the poor signal-to-noise ratio of the data prevents a reliable quantitative evaluation, one can estimate a decay time by order of magnitude. Both peaks are reduced by the same amount to about three quarters of the original intensity within the measurement time. Assuming exponential decay kinetics, this corresponds to a recombination time of ~4 ns. Thus, we can assume that within ten nanoseconds, the peaks have vanished, which would correspond to an emission rate of approximately 10^8 s^{-1}.

One conceivable mechanism for an N_s^- defect to lose its excess electron is by thermal excitation of its additional electron into the conduction band and the subsequent capture of that electron into an N_s^+ defect. The rate of this process would give an indication of the ionization energy of the N_s^- states and should increase with temperature. For that reason we performed a second set of measurements using identical parameters but with the sample at 450 K. No discernable difference was observed as compared to the room temperature case: no increase in the decay rate could be identified. However, the measured rate increase might be small and not be resolvable due to noise. In order to be distinguishable, the emission rate should at least double. This sets an upper limit for the energetic trap depth of the defect: the emission rate e_n is proportional to $e_n \sim \exp(-\Delta E/k_B T)$, where ΔE is the energy gap of the defect from the conduction band, i.e., its ionization energy and k_B is the Boltzmann constant. From this it follows that the rate increase from 300 to 450 K is less than twofold when ΔE is only 50 meV or less. Thus, thermal ionization can only be responsible for charge neutralization if the N_s^- defect is shallow with a ΔE of less than 50 meV.

The existence of an acceptor level less than 50 meV from the conduction band is however at variance with earlier work,[8] which suggested the N_s^- defect was responsible for the ~4.5 eV (270 nm) optical absorption band [see Fig. 1(a)] commonly observed in type Ib diamond, the transition occurring from the valence band to the defect state. Given the 5.5-eV band gap, this would lead to an acceptor level around 1 eV below the conduction band. Either this assignment is wrong, and an alternative mechanism is involved in the 270-nm band, or other recombination mechanisms, e.g., Auger processes, are taking

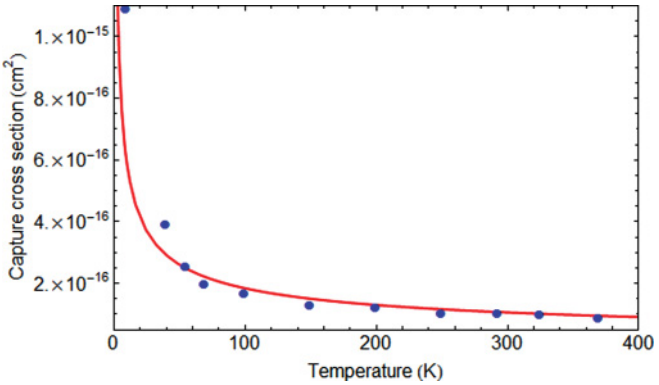

FIG. 5. (Color online) Measured temperature dependence of the capture cross section for the recombination of electrons into N_s^0 defect states (blue dots). The red line represents the fit to the MPE model described in the text.

place, which lead to a temperature-independent recombination time. Concluding, with the currently available data, we cannot draw any definitive conclusion about the mechanism that compensates the excess charges.

The presented data suggest that most electrons recombine with neutral N_s defects at low excitation densities. One can thus obtain a measure of the charge carrier capture cross section σ of the N_s^0 defect and its temperature dependence by relating the N_s defect concentration to the recombination time measured in the terahertz experiments:

$$\sigma = \frac{1}{N_s \nu \tau_r} \tag{2}$$

Here, N_s denotes the concentration of single substitutional nitrogen, ν the thermal electron velocity (given by $\nu = (3k_B T/m^*)^{1/2}$) and τ_r the recombination time. The obtained capture cross sections for all three investigated samples closely resemble each other. For reasons of clarity, we only plot the capture cross sections of the 150-ppm sample, shown as blue dots in Fig. 5.

The variation of the deduced capture cross section with temperature gives an indication of the relaxation mechanism of carriers back to N_s^0 sites. Neutral single substitutional nitrogen defects are known to lie 1.7 eV below the conduction band.[38] One possibility for the electron to lose the 1.7-eV excess potential energy, while relaxing back to the defect is via the emission of photons. The observed picosecond time scale of the relaxation process however renders this picture unlikely: luminescence lifetimes in diamond are at least in the nanosecond range, and no luminescence has been reported so far in the anticipated energy range.

The longitudinal optical phonon energy of diamond is 165 meV.[39] A direct recombination process to the ground state would thus require the simultaneous emission of ten phonons. While this would seem to result in very low capture cross sections, it was shown by calculations in the 1970s that significant lattice distortions can facilitate the phonon emission.[40,41] These first models were able to describe charge carrier recombination via multiphonon emission (MPE) with reasonably high capture cross sections.

In order to describe our data, we apply a simplified analytical MPE model as presented in Ref. 42. This model

essentially depends on three parameters: the Huang-Rhys factor S to describe the electron-phonon coupling strength of the transition, the energy E_{ph} of the phonon involved in the transition, and the energetic position E_T of the defect with respect to the conduction band. We set E_T=1.7 eV, the ionization energy of N_s^0. It is reasonable to assume that primarily LO phonons are involved in the transition because their energy is larger than acoustical phonons and coupling to electrons more efficient. The red line in Fig. 5 shows the fit that was obtained with $S = 10.1$. The Huang-Rhys factor S essentially quantifies the number of phonons emitted during the transition. Thus our obtained value makes physical sense since about ten LO phonons of 0.165-eV energy have to be emitted to cover the 1.7-eV energy difference. We note that in the model, E_{ph} is primarily determining the temperature dependence of the capture cross section. The simulations show that for large values of E_{ph}, as is the case for diamond (165 meV), σ is continuously decreasing with increasing temperature. For a phonon energy below 100 meV, the model predicts that the capture cross section starts to increase above room temperature, and for values below 50 meV, it is increasing with temperature over the whole temperature range. The values of E_T and S mainly influence the magnitude of the carrier capture cross section and are to some degree interchangeable over certain intervals. Reasonable fits can thus be obtained for a number of combinations of E_T and S. The values we obtain are physically reasonable and provide a good description to the data.

Our findings are directly relevant for understanding and controlling the lifetime and mobility of free carriers in diamond. Particularly in defect-rich materials that possess rapid recombination channels like the type Ib diamonds investigated here, photocurrent techniques that rely on charge collection might not be fast enough. The ability of time-resolved terahertz spectroscopy to take conductivity "snapshots" at any point after photoexcitation permits the direct and unambiguous assessment of figures of merit such as the charge carrier lifetime and mobility in such systems. In the emerging field of spintronics, negatively charged nitrogen vacancy defects (NV^-) are a promising candidate for room-temperature spin manipulation. Their performance is currently restricted by luminescence blinking, which is likely caused by charge state conversion. The demonstrated capability of single substitutional nitrogen defects, which are always present in samples containing nitrogen-vacancy centers, to act as electron acceptor states may be important in explaining the blinking of NV^- centers, as electron capture by neighboring N_s^0 defects could possibly neutralize NV^- centers.

IV. CONCLUSIONS

In conclusion, we have measured the picosecond dynamics of electrons excited from single substitutional nitrogen states into the conduction band in type Ib diamond using ultrafast pump-probe spectroscopy. Excitation densities were kept such that approximately only 1 out of 10^5 nitrogen defects were ionized. Using time-resolved terahertz spectroscopy, the electron mobility was deduced, and electrons were found to relax from the conduction band within tens of picoseconds. The results indicated that electrons in the conduction band scatter mainly from neutral nitrogen defects, showing mobilities that are largely independent of temperature. Furthermore, the recombination dynamics suggested that electrons predominantly relax from the conduction band into neutral nitrogen states rather than the original, ionized nitrogen defects (N_s^+). The application of a multiphonon emission model showed that this relaxation process is facilitated by the simultaneous emission of ten LO phonons. After all electrons have recombined, uncompensated N_s^+ and newly created N_s^- defects are present. The existence of the charged defects was confirmed by transient IR measurements. These measurements showed an absorption peak at 1332 cm^{-1} originating from the LVM of N_s^+ and a hitherto unknown absorption peak at 1349 cm^{-1} that is assigned to the LVM of N_s^-. The spectral position is in good agreement with density-functional calculations on the LVM of N_s^-. Our findings thus confirm that single substitutional nitrogen defects can act as electron acceptor states. The charged nitrogen defects are neutralized within approximately 10 ns. This relatively short lifetime may also explain why the negatively charged nitrogen defects have not been observed previously in steady-state optical measurements.

ACKNOWLEDGMENTS

The work is part of the research program of the Foundation for Fundamental Research on Matter, which is financially supported by the Dutch organization for Scientific Research (NWO). This work has been financially supported by the European Union Marie Curie Program (MEST-CT-2005-021000).

*Corresponding author: bonn@mpip-mainz.mpg.de

[1] M. Suzuki, H. Yoshida, N. Sakuma, T. Ono, T. Sakai, M. Ogura, H. Okushi, and S. Koizumi, Diam. Relat. Mater. **13**, 198 (2004).

[2] N. Tranchant, M. Nesladek, D. Tromson, Z. Remes, A. Bogdan, and P. Bergonzo, Physica Status Solidi a-Applications and Materials Science **204**, 3023 (2007).

[3] C. J. H. Wort and R. S. Balmer, Materials Today **11**, 22 (2008).

[4] J. Isberg, J. Hammersberg, E. Johansson, T. Wikstrom, D. J. Twitchen, A. J. Whitehead, S. E. Coe, and G. A. Scarsbrook, Science **297**, 1670 (2002).

[5] F. J. Heremans, G. D. Fuchs, C. F. Wang, R. Hanson, and D. D. Awschalom, Appl. Phys. Lett. **94**, 152102 (2009).

[6] S. C. Benjamin, B. W. Lovett, and J. M. Smith, Laser & Photonics Reviews **3**, 556 (2009).

[7] F. Jelezko and J. Wrachtrup, Physica Status Solidi a-Applications and Materials Science **203**, 3207 (2006).

[8] R. Jones, J. P. Goss, and P. R. Briddon, Phys. Rev. B **80**, 033205 (2009).

[9] S. Koizumi and M. Suzuki, Physica Status Solidi a-Applications and Materials Science **203**, 3358 (2006).

[10] F. De Weerdt and J. Van Royen, Diam. Relat. Mater. **10**, 474 (2001).

[11] P. U. Jepsen, D. G. Cooke, and M. Koch, Laser & Photonics Reviews **5**, 124 (2011).

[12] R. Ulbricht, E. Hendry, J. Shan, T. F. Heinz, and M. Bonn, Rev. Mod. Phys. **83**, 543 (2011).

[13]A. Nahata, D. H. Auston, T. F. Heinz, and C. J. Wu, Appl. Phys. Lett. **68**, 150 (1996).
[14]R. Jones and P. R. Briddon, *Identification of defects in semiconductors, Vol. 51A of Semiconductors and Semimetals* (Academic Press, Boston, 1998).
[15]M. J. Rayson and P. R. Briddon, Comput. Phys. Commun. **178**, 128 (2008).
[16]J. P. Perdew and Y. Wang, Phys. Rev. B **45**, 13244 (1992).
[17]J. P. Perdew, K. Burke, and M. Ernzerhof, Phys. Rev. Lett. **77**, 3865 (1996).
[18]J. P. Goss, M. J. Shaw, and P. R. Briddon, *Theory of Defects in Semiconductors* (Springer, Berlin/Heidelberg, 2007).
[19]C. Hartwigsen, S. Goedecker, and J. Hutter, Phys. Rev. B **58**, 3641 (1998).
[20]D. A. Liberman, Phys. Rev. B **62**, 6851 (2000).
[21]J. P. Goss, P. R. Briddon, R. Jones, and S. Sque, Diam. Relat. Mater. **13**, 684 (2004).
[22]H. J. Monkhorst and J. D. Pack, Phys. Rev. B **13**, 5188 (1976).
[23]E. Hendry, M. Koeberg, J. M. Schins, H. K. Nienhuys, V. Sundstrom, L. D. A. Siebbeles, and M. Bonn, Phys. Rev. B **71**, 125201 (2005).
[24]P. Drude, Annalen der Physik **308**, 369 (1900).
[25]F. Nava, C. Canali, C. Jacoboni, L. Reggiani, and S. F. Kozlov, Solid State Commun. **33**, 475 (1980).
[26]A. G. Redfield, Phys. Rev. **94**, 526 (1954).
[27]T. Malinauskas, K. Jarasiunas, E. Ivakin, N. Tranchant, and M. Nesladek, Physica Status Solidi a-Applications and Materials Science **207**, 2058 (2010).
[28]V. F. Gantmakher and Y. B. Levinson, *Carrier Scattering in Metals and Semiconductors* (Elsevier Science Ltd, Amsterdam, 1987).
[29]C. Erginsoy, Phys. Rev. **79**, 1013 (1950).
[30]K. Tsukioka and H. Okushi, Japanese Journal of Applied Physics Part 1-Regular Papers Brief Communications & Review Papers **45**, 8571 (2006).
[31]T. Malinauskas, K. Jarasiunas, E. Ivakin, V. Ralchenko, A. Gontar, and S. Ivakhnenko, Diam. Relat. Mater. **17**, 1212 (2008).
[32]P. T. Landsberg, *Recombination in semiconductors* (Cambridge University Press, Cambridge, 2003).
[33]S. C. Lawson, D. Fisher, D. C. Hunt, and M. E. Newton, J. Phys. Condens. Matter **10**, 6171 (1998).
[34]U. Fano, Phys. Rev. **124**, 1866 (1961).
[35]P. R. Briddon, Mater. Sci. Forum **83-87**, 457 (1992).
[36]A. T. Collins, P. J. Woad, G. S. Woods, and H. Kanda, Diam. Relat. Mater. **2**, 136 (1993).
[37]J. P. Goss, R. Jones, and P. R. Briddon, Phys. Rev. B **65**, 035203 (2001).
[38]R. G. Farrer, Solid State Commun. **7**, 685 (1969).
[39]S. A. Solin and A. K. Ramdas, Phys. Rev. B **1**, 1687 (1970).
[40]C. H. Henry and D. V. Lang, Phys. Rev. B **15**, 989 (1977).
[41]D. V. Lang and C. H. Henry, Phys. Rev. Lett. **35**, 1525 (1975).
[42]J. H. Zheng, H. S. Tan, and S. C. Ng, J. Phys. Condens. Matter **6**, 1695 (1994).